

REPORT DOCUMENTATION PAGE			Form Approved OMB No. 0704-0188	
<small>PUBLIC RELEASE STATEMENT: This document contains information which is exempt from release under the provisions of the Freedom of Information Act (5 U.S.C. 552). This document is being released to the public in accordance with the provisions of the Act. The release of this document is not intended to constitute an official Department of Defense position, policy or decision unless otherwise documented. This document is being released to the public in accordance with the provisions of the Act. The release of this document is not intended to constitute an official Department of Defense position, policy or decision unless otherwise documented. This document is being released to the public in accordance with the provisions of the Act. The release of this document is not intended to constitute an official Department of Defense position, policy or decision unless otherwise documented.</small>				
1. AGENCY USE ONLY (Leave blank)		2. REPORT DATE	3. REPORT TYPE AND DATES COVERED Final 9-15-93 to 9-14-96	
4. TITLE AND SUBTITLE Sensors for In-Situ Process Monitoring and Process Control			5. FUNDING NUMBERS F49620-93-1-0592	
6. AUTHOR(S) B. T. Khuri-Yakub Krishna C. Saraswat				
7. PERFORMING ORGANIZATION NAME(S) AND ADDRESS(ES) Edward L. Ginzton Laboratory Stanford University Stanford, CA 94305-4085			8. PERFORMING ORGANIZATION REPORT NUMBER G.L. 5497	
9. SPONSORING / MONITORING AGENCY NAME(S) AND ADDRESS(ES) AFOSR/NM 110 Duncan Avenue, Suite B115 Bolling AFB, DC 20332-0001			10. SPONSORING / MONITORING AGENCY REPORT NUMBER	
11. SUPPLEMENTARY NOTES The views, opinions and/or findings contained in this report are those of the authors and should not be construed as an official Department of Defense position, policy or decision unless otherwise documented.				
12a. DISTRIBUTION / AVAILABILITY STATEMENT Approved for public release; distribution unlimited.			12b. DISTRIBUTION CODE	
13. ABSTRACT (Maximum 200 words) This report presents the results of the development of an ultrasonic sensor for in-situ monitoring of silicon wafer temperature. The sensor is based on the measurement of the velocity of ultrasonic Lamb waves in the wafer, and relating this velocity to temperature. We present a method for efficient excitation and detection of Lamb waves in the wafer, a theoretical model for relating the variation of velocity as a function of temperature, and an electronic implementation for the sensor. Our results indicate the ability to measure the temperature with an accuracy of 1°C in most integrated circuit processing environments. The sensor has also been used in a tomographic configuration to allow the measurement of spatial distribution of temperature. Finally, we highlight the potential for simultaneous measurement of temperature and film thickness in-situ.				
14. SUBJECT TERMS Temperature, Film Thickness, Ultrasonic, Lamb Waves, Time of Flight, Spatial Distribution.			15. NUMBER OF PAGES 29	
			16. PRICE CODE NTIS only	
17. SECURITY CLASSIFICATION OF REPORT Unclassified	18. SECURITY CLASSIFICATION OF THIS PAGE Unclassified	19. SECURITY CLASSIFICATION OF ABSTRACT Unclassified	20. LIMITATION OF ABSTRACT SAR	

Sensors for In-Situ Process Monitoring and Process Control

Final Report

September 15, 1993 to September 14, 1996

AFOSR -1-
Grant F49620-93-0592

G. L. Report No. 5497

Principal Investigators

Krishna C. Saraswat
B. T. Khuri-Yakub

Edward L. Ginzton Laboratory
Stanford University
Stanford, California 94305-4085

19971006 167

Ultrasonic *in - situ* wafer temperature sensor for semiconductor processing

1 Introduction

Temperature is one of the most common and important process parameters in semiconductor manufacturing. A search in Stanford University Library database INSPEC with subject key words "temperature and semiconductor processing" results in over 2700 scientific articles in a subset of engineering and physics publications in the last 8 years. Especially, accurate measurement of wafer temperature and its spatial distribution become critical as the tolerances in device dimensions get tighter [18]. These concerns define the properties of the desired temperature sensor for semiconductor processing. The required measurement accuracy of the temperature sensor is around $\pm 1^\circ\text{C}$ for many processes [10]. The sensor should be able to measure temperature with this accuracy in the -100°C to 1200°C range for different processes. Due to contamination and temperature uniformity concerns, non-contact temperature measurement methods are preferred. Real-time, *in - situ* sensors are required for real-time closed loop control of wafer temperature. Furthermore, information on temperature uniformity is essential especially for processing of wafers with 20 cm or larger diameter.

Currently, optical pyrometry is the dominant technique for temperature measurement in the semiconductor industry. In pyrometry, radiation from the wafer is used to measure its temperature in a non-contact fashion [20]. This type of temperature measurement is typically at a single point on the wafer with an accuracy that is limited by variations in wafer emissivity during processing and interference from other light sources [25, 26, 27]. There are emissivity correction methods, but they are generally complex and costly [5]. Another major problem with pyrometry is the lack of sensitivity at low temperatures, since the radiated power from the wafer is proportional to the fourth power of its temperature. This limits the use of pyrometers to process temperatures higher than 400°C , which is not acceptable for many processing steps. Since thermocouples cause contamination and temperature non uniformity during thermal processing, thermocouples attached at different locations on the wafer can only be used for calibration purposes. Approaches utilizing thermal expansion measurements provide average wafer temperature with low accuracy and require special reflective structures on the wafer [3, 19]. Ellipsometry is also used for simultaneous oxide film thickness and temperature measurements [21]. This technique is limited to dielectric films only, and the temperature accuracy is limited to $\pm 20^\circ\text{C}$.

The use of ultrasonic waves for wafer temperature measurement was initiated and

realized at Stanford University by Lee and co-workers [13, 10]. In that study, laser ultrasound techniques were used to generate and detect acoustic waves both in the wafer and its immediate ambient. Although, in principle, the method should be able to measure wafer temperature accurately, the required SNR is difficult to achieve. To overcome this difficulty, the ultrasonic wafer temperature sensor (UTS) using Hertzian contact transducers for A_o mode Lamb wave excitation was also first demonstrated by the same group [10, 11, 12]. The already existing quartz support pins were modified to act as Hertzian contact transducers. UTS can also be considered as a “non contact” technique since it does not require any “additional” contact to the wafer in single wafer processing systems. A time-of-flight (TOF) measurement technique was used to infer wafer temperature *in-situ* in a rapid thermal processing (RTP) environment with $\pm 5^\circ\text{C}$ accuracy relying on calibration with thermocouples.

In this report, we calculate the temperature sensitivity of the A_o mode Lamb waves in wafers of typical semiconductor processing materials. We also discuss the effect of thin films on the A_o mode Lamb wave propagation and their temperature sensitivity. We show that for some thin film materials, there are critical frequencies where the thin film sensitivity is minimized. This information proved to be useful for simultaneous film thickness and temperature measurements [17, 16]. We describe the implementation and integration of UTS to the rapid thermal multiprocessor (RTM) at Stanford University. As an example, we describe the use of UTS for *in-situ* temperature and crystallinity monitoring in the manufacture of thin film transistors for flat panel displays. We also present results of *in-situ* wafer temperature tomography using 8 spring loaded sensors and a 3 zone tomography system for the RTM.

2 Temperature sensitivity of the A_o mode Lamb waves

In order to understand and optimize the UTS, one should investigate the temperature sensitivity of the A_o mode Lamb wave and its dependence on various parameters. These parameters include the frequency of operation, wafer dimensions, thin film coatings of different materials, wafer material anisotropy, wafer surface roughness and topology. A few of these factors were examined in a previous study [10]. However, the Lamb wave theory used in that study assumes that the wafer material is isotropic. Also, the effect of thin films on the wafer were included via an approximate perturbation approach.

We base our exact calculations on the surface impedance approach discussed in [?]. One of the advantages of the UTS is that it can be used with different semiconductor wafer materials without any modification. Since the measurement is based on mechanical

properties only, optical (transparency, emissivity etc.), electrical (doping density etc.) properties do not affect the measurements [8]. As the most common wafer materials, we calculate the temperature sensitivity for silicon, gallium arsenide and quartz/glass wafers. In Fig. 1, we plot the temperature sensitivity of phase velocity ($\frac{dV_p}{V_p dT}$) of the A_o mode as a function of fd for these materials. The effect of temperature is included in the calculations using the measured temperature coefficients. For silicon and fused quartz we use the data from McSkimmin, and for gallium arsenide we use the data from Garland et al. as compiled in table 2 [14, 7]. For silicon and gallium arsenide, the calculations are done assuming propagation in $\langle 100 \rangle$ direction on the (001) surface of wafers. The temperature coefficient k_{12} for isotropic materials can be obtained using the relation $c_{12} = c_{11} - 2c_{44}$.

Material	k_{11} (1/ $^{\circ}$ C)	k_{44} (1/ $^{\circ}$ C)	k_{12} (1/ $^{\circ}$ C)
Silicon	-6.75×10^{-5}	-4.4×10^{-5}	-9.95×10^{-5}
GaAs	-1.5221×10^{-4}	-3.78×10^{-5}	-2.87×10^{-4}
Fused quartz	$+2.32 \times 10^{-4}$	$+1.45 \times 10^{-4}$	
Aluminum	-2.796×10^{-4}	-5.11×10^{-4}	

Table 1: Temperature coefficients of elastic constants of common semiconductor materials. The temperature dependent constants are calculated by the equation $c_{ij}(T) = c_{ij}(T_o)(1 + k_{ij}(T - T_o))$.

The sensitivity figures are calculated at 20 $^{\circ}$ C, and found to be of the order of 10 $^{-5}$ / $^{\circ}$ C for all three materials. Fused quartz has a positive temperature coefficient in contrast with silicon and gallium arsenide, in which the phase velocity of Lamb wave decreases with increasing temperature. Although the sensitivity figures are small, they are nearly an order of magnitude larger than the corresponding thermal expansion coefficients [15]. These curves also suggest that at a given frequency, the wafer thickness variations do not affect the temperature coefficient significantly. However, wafer thickness variations cause shifts in the temperature measurement by UTS due to phase velocity dispersion. These shifts can be corrected if the initial process temperature is known.

We also examine the effect of anisotropy on the temperature coefficient by calculating its variation with propagation direction of Lamb waves. The results for (001)-cut silicon and gallium arsenide at $fd = 0.1$ MHz-mm are shown in Fig. 2. The four fold symmetry of these materials on this plane is also observed in the temperature sensitivity. The maximum variation is 5.5% and 13% for silicon and gallium arsenide, respectively. These results show that the alignment of measurement direction is important to minimize the effect of wafer alignment on temperature measurements.

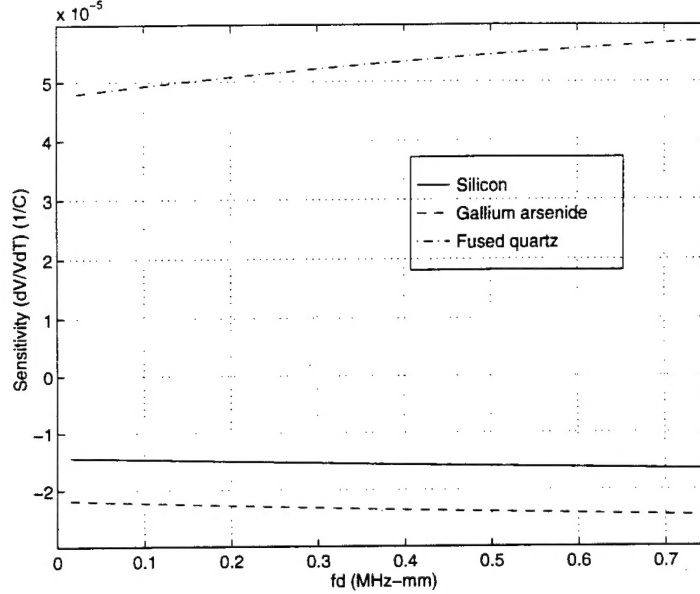


Figure 1: Absolute temperature sensitivity of the A_0 mode phase velocity for different semiconductor wafer materials.

2.1 Effect of thin films and wafer roughness

In many semiconductor processing steps, one or more thin layers are present or being deposited on the wafers. These films affect the phase velocity of the Lamb waves propagating in the relatively thick semiconductor wafer. It is possible to exploit this sensitivity to measure the thickness and other properties of these films [17]. To investigate the effects of thin films on Lamb wave propagation in wafers we use the surface impedance approach. We use the elastic properties of film materials tabulated in Simmons and Wang [6]. Fig. 3 shows the A_0 mode Lamb wave phase velocity variation in a 0.5 mm thick (001) silicon wafer as a function of film thickness. These film materials are commonly used in semiconductor processing. The propagation is in $\langle 100 \rangle$ direction at $f=200$ kHz. The phase velocity variation is linear in this film thickness range, since the film is a small perturbation on the much thicker silicon wafer. Aluminum and silicon dioxide have elastic properties similar to silicon, and their main effect is to increase thickness in this small perturbation regime. With its high density (7.9 gr/cm^3), the copper film loads the silicon wafer, therefore decreases the phase velocity with a $-0.6 \text{ m/sec}/\mu\text{m}$ rate. Silicon nitride is harder than silicon with a comparable density. Hence, silicon nitride film stiffens the silicon wafer with $2.8 \text{ m/sec}/\mu\text{m}$ change in phase velocity. The results indicate that the density and shear elastic constant (c_{44}) of the film material relative to silicon dominate the change in the phase velocity. This is expected

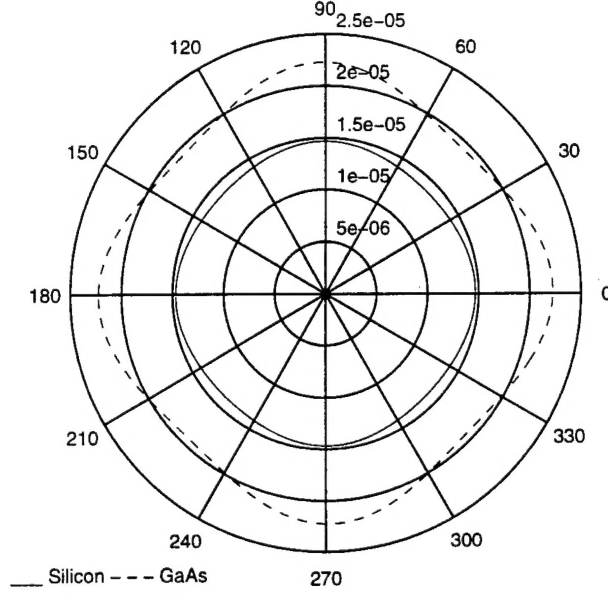


Figure 2: Variation of absolute temperature sensitivity of A_0 mode phase velocity with measurement direction on (100)-cut silicon and GaAs wafers. The wafer thickness is 0.5 mm and the frequency is 200 kHz.

due to the shear nature of the A_0 mode, which is predominantly a flexural wave in this fd range.

Thin film sensitivity ($\frac{dV_p}{V_p dh}$) of the A_0 mode Lamb wave is also a function of frequency due to its dispersive nature and the multilayered waveguide structure. In Fig. 4 we plot this variation as a function of fd , where d denotes the silicon wafer thickness. The sensitivity is calculated assuming a 500 Å film deposition on the wafer ($dh = 500$ Å). Silicon nitride and copper films stiffen and load the wafer, respectively in the whole frequency range. For aluminum and silicon dioxide films, the phase velocity sensitivity is negligible around $fd = 0.8$ MHz-mm and $fd = 3.2$ MHz-mm, respectively. At low frequencies, these films have the effect of increasing the wafer thickness, hence increasing the phase velocity due to dispersion. At high frequencies, the acoustic energy is concentrated more at the surfaces and the slower phase velocity of the films start to dominate as predicted by perturbation theory [2]. These fd regions can be used to minimize thin film effects during temperature measurements for these particular materials. Also, noting that the temperature sensitivity is a slowly varying function of frequency (Fig. 1), one can use Hertzian contact transducers operating at two different frequencies to simultaneously monitor both the temperature and thin film thickness. These predictions are verified by experiments in an aluminum sputtering station and *in-situ*

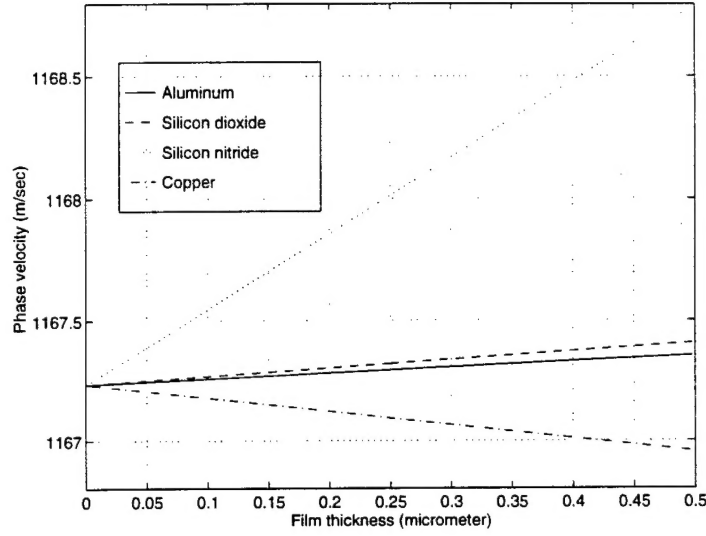


Figure 3: Calculated A_0 mode Lamb wave phase velocity variation with different film materials.

temperature and thin film thickness measurement is realized using transducers operating at 550 kHz and 1.5 MHz on 0.5 mm thick silicon wafers [16]. For the applications of the UTS, thin films have two different effects. The phase velocity variation due to the thin film causes an absolute shift of TOF measurements at constant temperature. In addition to that, the temperature sensitivity of the A_0 mode changes in the presence or during the growth of films with different thermal properties. We model the second effect by including the variation of thin film elastic constants with temperature in the calculations. Fig. 5 shows the results for silicon dioxide and aluminum films on a 0.5 mm thick silicon wafer at 200 kHz. The temperature sensitivity decreases by 1.4% for $1\mu\text{m}$ of silicon dioxide film. In case of aluminum it increases by 2.2%. These changes are expected, considering the temperature coefficients of the film materials [6]. These results show that the cross coupling between the effects of thin films and the temperature is not significant. For practical cases of thin ($100\text{-}200\text{\AA}$) gate oxide deposition, the effect of the films can be neglected still achieving $\pm 1^\circ\text{C}$ temperature accuracy.

Wafer backside roughness is a problem for temperature measurement systems using pyrometry and optical detection due to emissivity and reflectivity variations [25]. To analyze the effects of surface roughness on the UTS, we use the perturbation approach [2]. Since the wavelength and the wafer thickness are much larger than the rms surface roughness, the perturbation approach is appropriate for calculations. The surface roughness causes an

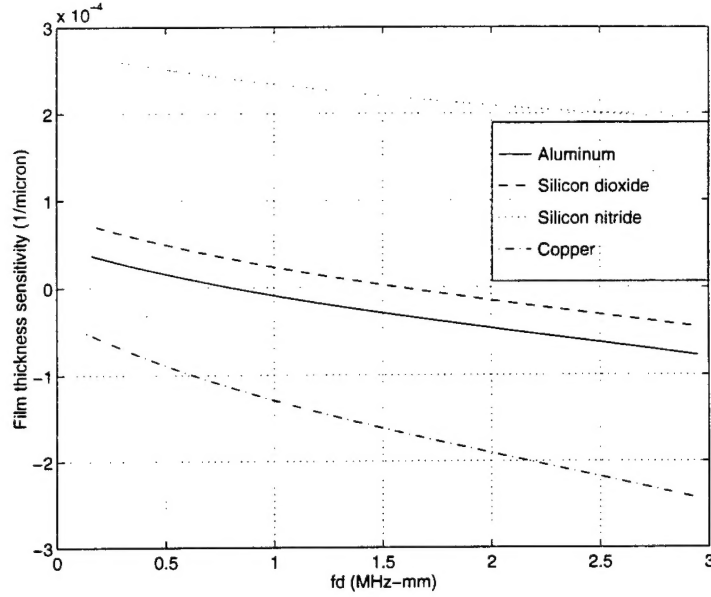


Figure 4: Calculated A_o mode Lamb wave phase velocity sensitivity as a function of frequency-thickness product for different film materials.

increase in phase velocity and also attenuates the Lamb wave. The results of the perturbation calculation of change in phase velocity changes are shown in Fig. 6, for 10 cm and 20 cm diameter silicon wafers with 0.5 mm and 0.725 mm thickness, respectively. These are typical dimensions of commercial semiconductor wafers. The operation frequency is 200 kHz and the wavelength of the Lamb wave is around 5-6 mm. The attenuation caused by the surface roughness is extremely small and is not plotted. The main temperature measurement error is due to phase velocity changes, which is smaller than 1×10^{-5} for rms surface roughness up to $10 \mu\text{m}$. The corresponding temperature difference is less than $\pm 1^\circ\text{C}$ for surface roughness variation up to $65 \mu\text{m}$. These figures suggest that the UTS is virtually independent of wafer roughness variations and hence surface topology.

3 Time of flight measurement method

A typical implementation of the UTS using Hertzian contact transducers is shown in Fig. 7. If the wafer is supported only by the quartz pins, the maximum number of transducers is limited to 3. In many semiconductor process chambers the wafer is held against a flat or slightly curved surface by mechanical or electrostatic clamping. In this case, more than 3

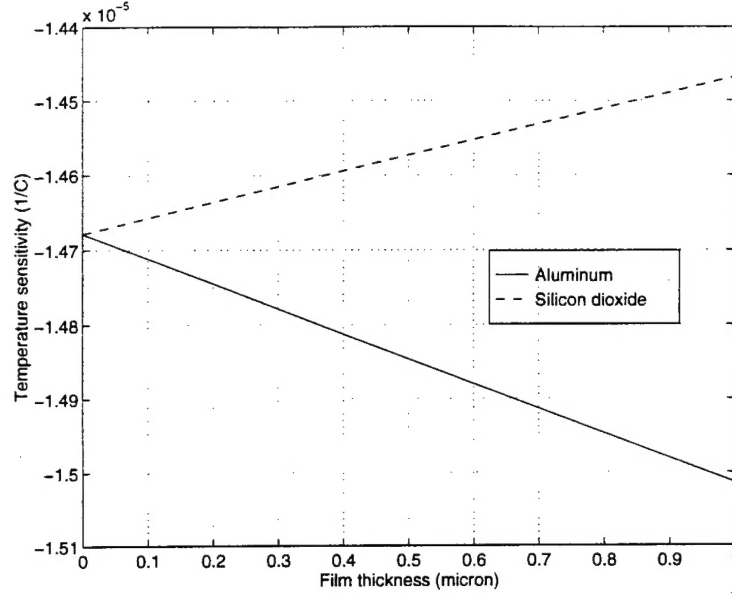


Figure 5: Calculated temperature sensitivity of A_0 mode Lamb wave phase velocity as a function of film thickness.

transducers can be used for average temperature measurement and its distribution on the wafer as we discuss in the following sections. In a typical temperature measurement cycle, one of the Hertzian contact transducers is used as a transmitter. A short duration ($< 1\mu\text{sec}$), high negative voltage pulse ($100\text{V} < |V_{\text{peak}}| < 1000\text{V}$) is applied to the transmitter to excite Lamb waves in the wafer. Since the Hertzian contact transducer is used in the low fd region, only the A_0 mode Lamb wave is excited. Most of the longitudinal wave excited in the quartz buffer rod is reflected from the tip of the transducer as an echo signal. A particular zero crossing in this signal is taken as the timing reference as shown in Fig. 8. The Lamb wave in the wafer travels from the transmitter to the receiver and is detected at the receiver transducer terminals and amplified by a pre-amplifier. Since the piezoelectric transducer has an electrical impedance of 1-10 k Ω , the pre-amplifier is designed to have a high input impedance and low input noise current. The TOF is then measured by a precision time interval counter between the time reference from the echo signal and a zero-crossing in the received signal. The zero-crossing selection is made by enabling the counter by TTL signals generated at the master timer. The TOF is read by the computer through the GPIB connection and converted to temperature using a theoretical calculation or an experimental calibration curve. The temperature sensitivity of the TOF technique is not equal to either the phase or the group velocity sensitivity. Although the wave packet travels with the group velocity, the zero crossing measurement depends on the phase velocity as well.

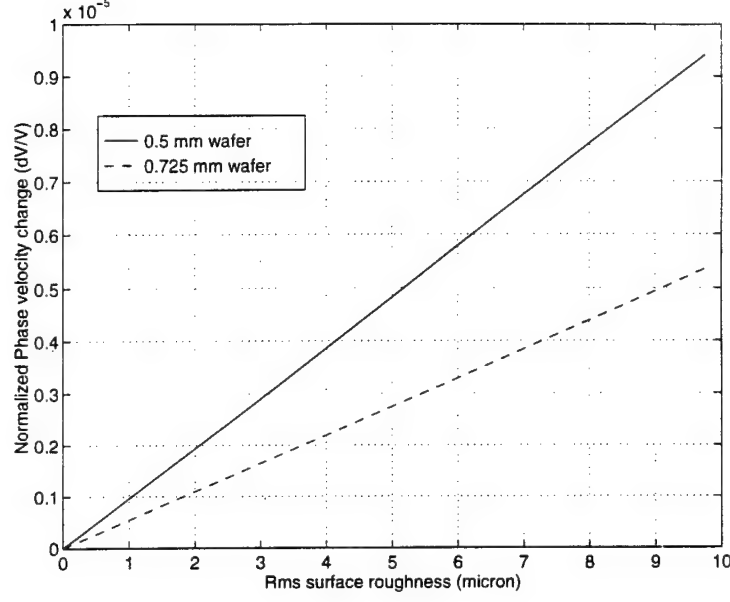


Figure 6: Normalized A_0 mode Lamb wave phase velocity change with rms surface roughness for 0.5 mm and 0.725 mm silicon wafers. Frequency is 200 kHz.

Given the the wide frequency spectrum of the pulse signals, it is logical to do the temperature sensitivity calculations directly on the signals in the frequency domain. To obtain the theoretical sensitivity, we assume that the Lamb wave signal that has a frequency spectrum of $S_t(f, r = 0)$ at the transmitter location, that is independent of temperature and can be calculated from the received signal spectrum at $T = T_o$. If the receiver is located more than 3 wavelengths away from the transmitter, we can use the far field assumption for the cylindrically diverging Lamb waves and write the frequency spectrum of the signal at $r = 0$ in terms of the signal at $r = r_o(T_o)$ as

$$S_t(f, r = 0) = S_r(f, T_o, r_o(T_o)) \sqrt{k(f, T_o) r_o(T_o)} e^{jk(f, T_o) r_o(T_o)} \quad (1)$$

To find the signal at the transmitter correctly, the wafer thickness and transmitter-receiver distances are obtained by external measurements and incorporated in the calculations. The temperature dependence of phase velocity is included in the wavenumber $k(f, T)$. Thermal expansion of the wafer is included in $r_o(T)$ using the published thermal expansion data [15]. The received signal at another temperature $T = T_1$ is calculated by propagating the spectrum back and taking the real part of the inverse Fourier transform

$$s_r(t, T_1, r_o(T_1)) = \text{Re}\{FT^{-1}\{S_t(f, r = 0) \frac{1}{\sqrt{k(f, T_1) r_o(T_1)}} e^{-jk(f, T_1) r_o(T_1)}\}\}. \quad (2)$$

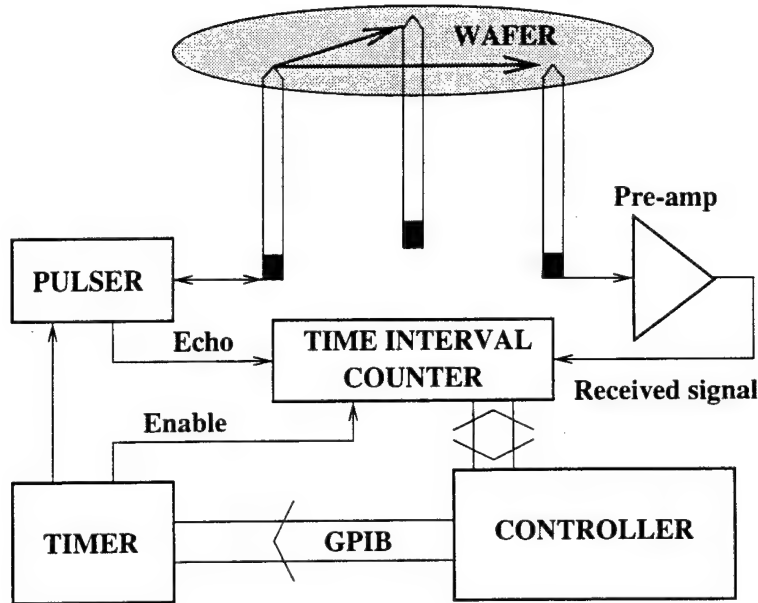


Figure 7: Computer controlled TOF measurement setup schematic.

The temperature sensitivity of a particular zero crossing in the received signal is found from these theoretical signals. Basically, it is assumed that all the temperature dependence during the process is confined to the Lamb wave propagation in the wafer. By taking the time reference from the echo signal it is assumed that the effect of heating of the buffer rods is eliminated. Even with these assumptions, good agreement is observed between the measured and predicted TOF sensitivities. In Fig. 9, a typical measured TOF vs. thermocouple temperature curve obtained in the RTM is shown along with the calculated curve. For the given signal and transmitter-receiver distance of 83.4 mm, the TOF sensitivity is calculated as 1.78 nsec/ $^{\circ}$ C. Part of the discrepancy in the curves is due to the non uniform temperature distribution of the wafer. The thermocouple measures the temperature at a single point, whereas the UTS gives the average temperature on the measurement path. The dependence of TOF on temperature is linear for all practical process temperature ranges, since the temperature coefficient is very small.

The procedure outlined above can be modified to include the effect of wafer thickness. The dependence of phase velocity on wafer thickness is a function of frequency and it is different than the temperature dependence. So, given sufficient SNR, both variables can be inverted using the information at different frequencies. The same argument is also valid for distance inversion.

The assumptions for the theoretical calculation may not be valid in some cases. For

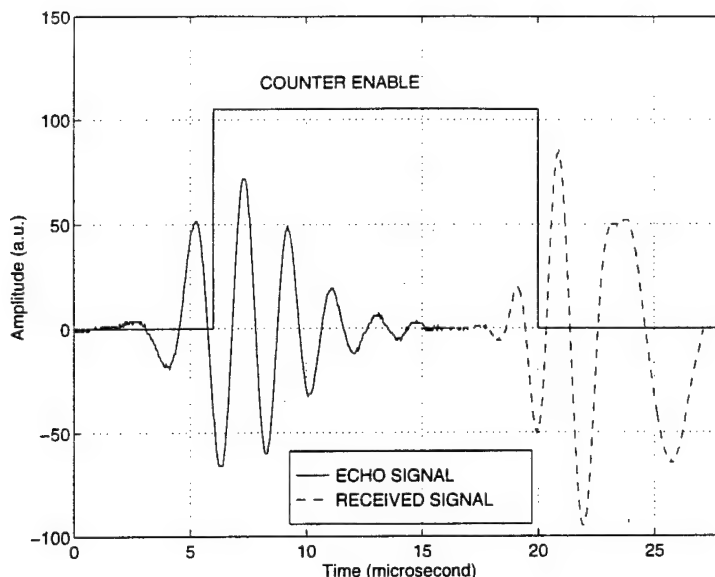


Figure 8: Timing diagram for selection of zero crossings in echo and received signals for TOF measurement. The transducers have center frequency of 500 kHz.

example, when the buffer rods are rapidly and unevenly heated, or there is humidity so that the Hertzian contact is significantly dependent on temperature, the calculated sensitivity may be in large error. In those cases an experimental calibration can be used. Experimental calibration is done by heating the wafer uniformly in several steps to the process temperature and recording the TOF as well as the temperature read by thermocouples attached to the wafer. Assuming that the process is repeatable, a look-up table or a polynomial fit can be used to convert TOF to temperature for *in-situ* temperature measurement. This calibration technique gives satisfactory results as will be discussed in the next section.

Given the small temperature coefficient of TOF measurement, high SNR is required for accurate temperature measurements. In Fig. 10, we plot a measured curve of the temperature accuracy of the UTS as a function of SNR. This curve is valid for a transmitter-receiver distance of 80 mm and a transducer operating around 200 kHz. The SNR is adjusted by increasing the force on the Hertzian contact. The same effect can be realized by increasing the radius of curvature at the tip of the buffer rod. The curve shows that in order to measure the wafer temperature with $\pm 1^\circ\text{C}$ accuracy, the SNR of the UTS should be larger than 50 dB. This figure is achieved with 10 cm wafers by Hertzian contact transducers with 10 cm tip radius and low noise electronics.

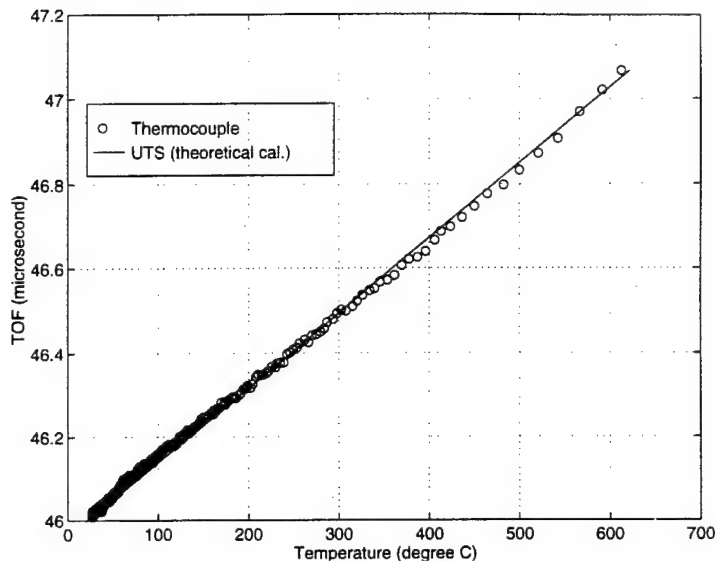


Figure 9: TOF vs. temperature curve for UTS and corresponding thermocouple readings.

4 Implementation in Stanford RTM

As an application platform for the UTS, we use the experimental RTM developed at the Center for Integrated Systems at Stanford University [22]. The schematic of the RTM is shown in Fig. 11. In this chamber, the wafer is supported by three fused quartz support pins and heated by a circularly symmetric three zone tungsten halogen lamps. The light flux is coupled to the wafer through a quartz window. To integrate the UTS in the RTM, some parts of the RTM have been modified. The main modification is the change of the base plate of the chamber to incorporate 3 Hertzian contact transducers in place of the support pins. This configuration provides excellent acoustical isolation and vacuum sealing. The base plate is water cooled to prevent heating of the piezoelectric transducer. The piezoelectric transducers are held outside the chamber, at room temperature. Due to the special structure of the chamber, which was not designed for the UTS, the 3 mm diameter quartz buffer rods have to be 22 cm long. This causes mechanical stability problems resulting in amplitude variations while the UTS is used with 10 cm wafers, whereas with 15 cm and 20 cm wafers, which are the industry standards, the mechanical stability is not a problem and SNR in excess of 50 dB is obtained with a tip radius of 10 cm.

In Fig. 12, TOF data collected at 10 Hz rate during a typical run is plotted. The corresponding thermocouple reading is plotted in Fig. 13. The data rate is mainly determined

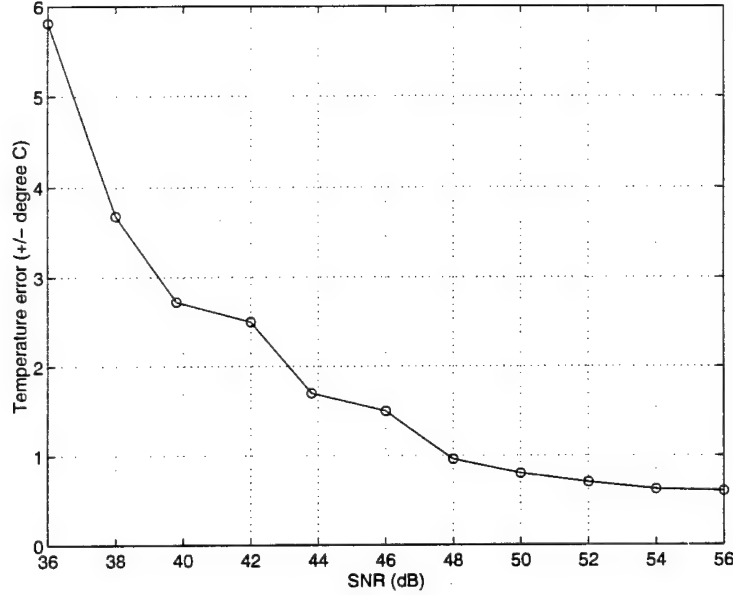


Figure 10: Estimated temperature error of the UTS as a function of SNR. During measurements SNR is varied by changing the force on the Hertzian contact.

by the decay rate of the Lamb waves in the wafer. At atmospheric pressures, a 10 Hz data rate which is desirable for in-situ control is easily achievable. The dynamic range of the UTS and the high SNR in the 20°C to 800°C range is evident from the curves. Again we note that the thermocouple indicates the temperature at the center of the wafer, whereas the ultrasonic sensor provides an average temperature.

The UTS is also incorporated in a real-time temperature control system. A single path TOF measurement is used to control the state of the wafer. Using experimental calibration, a single input single output controller is designed to track a TOF recipe [4]. The result of such a run is shown in Fig. 14. The dashed line represents the targeted TOF values, and the solid line is the actual data. The TOF data tracks the desired response in a closed control loop, again with a 10 Hz data rate.

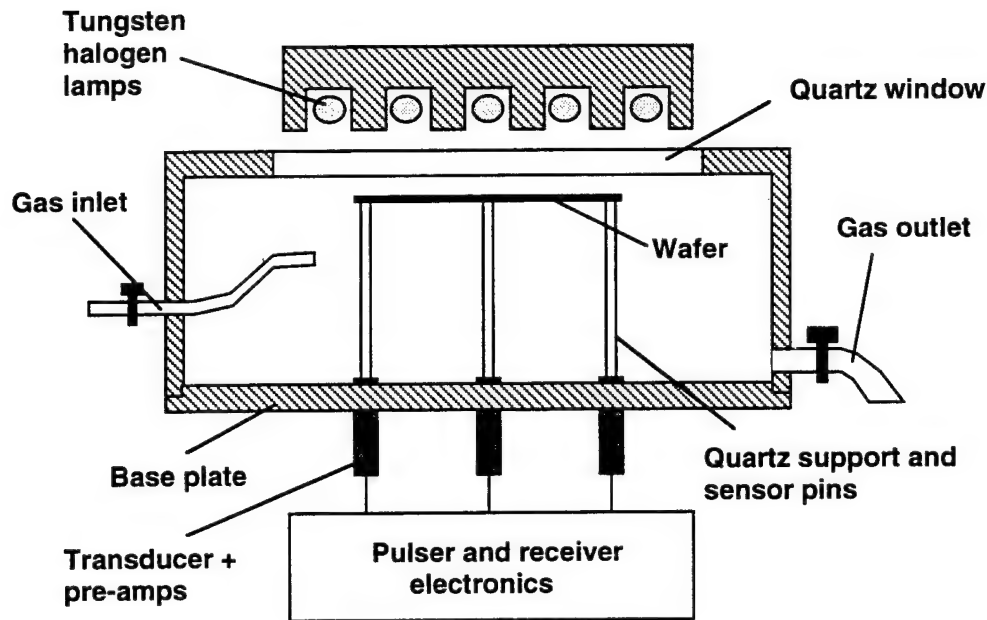


Figure 11: Schematic diagram of the RTM. Inside of the chamber remains unchanged after the integration of the UTS.

5 Application in *in-situ* temperature and crystallinity monitoring

Thin film transistors have extensive applications in active matrix liquid crystal displays. Fabrication of low temperature polysilicon thin film transistors for driver circuitry on low-cost glass display substrates will reduce the cost of these displays significantly [28]. Use of glass substrates imposes tight tolerances on the process temperature range. These materials begin to warp around 600°C, a condition that is not acceptable for display applications. To prevent warpage, it is necessary to limit the peak process temperature and minimize the thermal budget. Rapid thermal annealing (RTA) emerges as a solution to this problem [28, 9, 24]. Using RTA, high quality thin film transistors can be produced with high throughput. This requires an endpoint detection method that monitors the substrate temperature *in-situ*

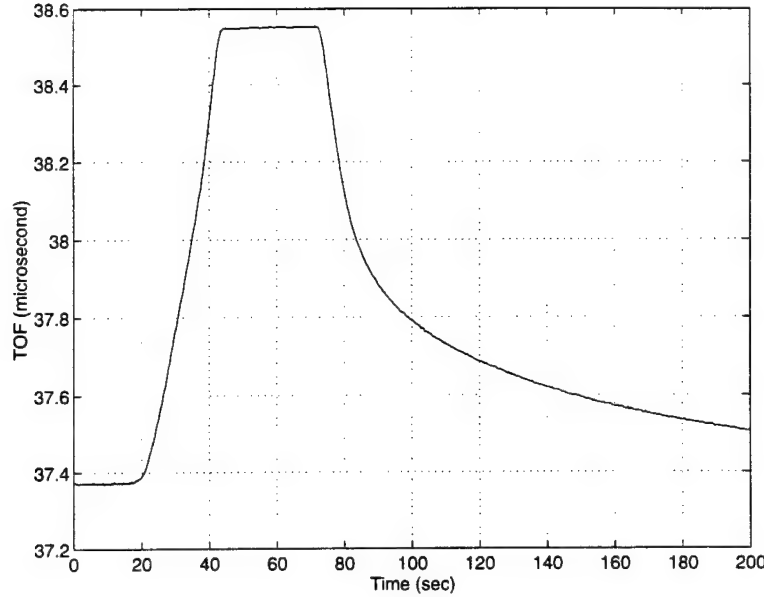


Figure 12: Measured TOF during a typical run in RTM. The corresponding thermocouple data is shown in Fig. 13.

and accurately.

As mentioned earlier, pyrometers are commonly used for temperature monitoring in RTA whose reading is depends on emissivity. The thin films present on the wafer surface are also known to affect the emissivity [27]. The film material, film thickness and crystallization phase of the film are important factors in determining the emissivity. During the RTA of thin films on transparent substrates, such as glass, crystalline phase transitions take place, resulting in significant emissivity variations. Consequently, a method which is particularly insensitive to emissivity is required. Since UTS is virtually independent of optical properties of the wafer, it enables isolation of emissivity variations from the temperature measurements. Since emissivity variations due to phase transitions determine the heating profile, UTS provides crystallinity information through accurate temperature measurements.

We used quartz wafers as substrates for crystallinity monitoring experiments. The substrates are coated with thin (100-150 nm) amorphous silicon films. Since the films are very thin as compared to the 0.5 mm thick substrates, the UTS basically measures the substrate temperature. However, since in the RTM and most RTA chambers the wafers are heated by a lamp, the thin films dominate the heating profile. The optical absorption coefficient of thin amorphous films is higher than the absorption of a polysilicon film. Hence, amorphous films are more opaque than polycrystalline films of the same thickness. Because of this,

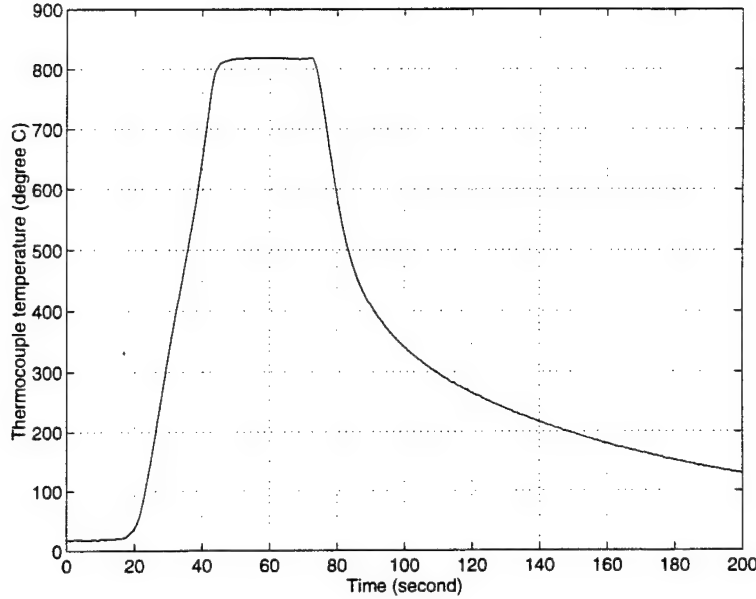


Figure 13: Wafer temperature measured by the thermocouple attached to the wafer during the same run as in Fig. 12. The temperature varies from room temperature to more than 800°C.

the absorption of light by the film drops drastically during the amorphous-polycrystalline phase transition. Since, the quartz/glass substrates are transparent to the lamp radiation, the crystal phase of the films determine the substrate temperature.

To monitor thin film crystallization during RTA, the UTS is used for *in-situ* temperature measurements and hence control crystalline phase transitions. In contrast to silicon wafers, thermocouples can not be used even for experimental calibration, because they affect the temperature distribution significantly. Therefore, the temperature coefficients of the particular quartz wafers are obtained by TOF experiments in an oven. The temperature sensitivity of TOF for two particular zero crossings in the received signal are found from the slope of TOF vs. temperature curves in the 20–75°C range. The temperature range is limited to prevent the piezoelectric transducers from depoling. Using these experimental data, the temperature coefficients of the elastic constants of the quartz substrate are inverted using Eq. 1 and 2 in a MATLAB optimization routine. The error in these coefficients is estimated to be 4% due to temperature dependence of PZT transducers and distance measurements. With these parameters, the UTS has a TOF sensitivity of -3.11 nsec/°C for measurements on quartz wafers in the RTM.

A typical temperature profile measured by the UTS during the RTA of a quartz wafer is

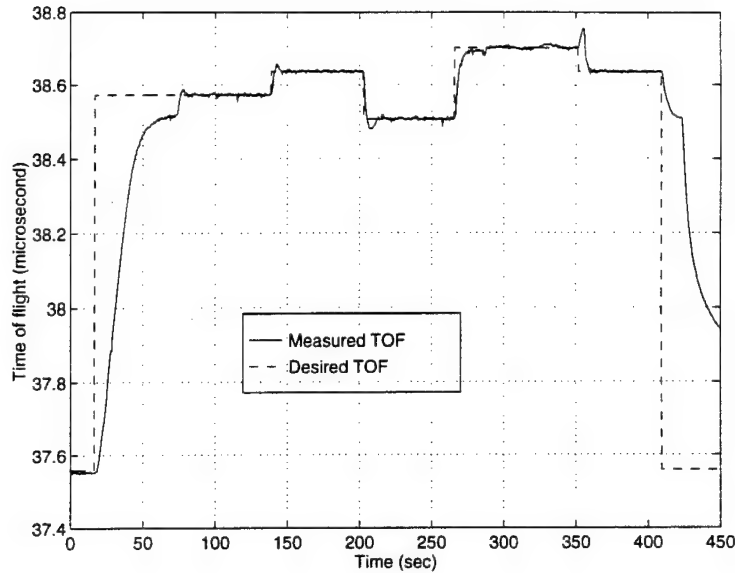


Figure 14: Measured TOF during a real time controlled recipe run. The controller is active from $t=70$ sec to $t=400$ sec.

shown in Fig. 15. At the start of the first run, the thin film is amorphous. The temperature clearly drops at the amorphous-polycrystalline transition although the input light flux is kept constant. In the consequent run, the film which is initially polycrystalline does not have this peculiar temperature drop and does not heat up as much as the amorphous film. This verifies the higher light absorption of the silicon film in amorphous phase. The peak temperature during RTA is measured to be 588°C with 12°C standard deviation in 6 different runs. Thus, the temperature repeatability is around 2%. These figures are $10\text{-}25^{\circ}$ less than the published data on the RTA of quartz wafers [9]. We note that the UTS measures average wafer temperature along the measurement path. Also the RTM lamp is designed for silicon substrates and uniformity is not optimal for quartz substrates. Because of this the temperature distribution during RTA is clearly not uniform as evidenced by visual inspection of the wafers.

To correlate the temperature measured by the UTS and the crystalline phase transitions, the process is stopped at points A,B and C as shown in Fig. 15. Transmission electron microscopy (TEM) micrographs of the corresponding films are shown in Fig. 16, 17, 18. At point A, the film is completely amorphous and the electron diffraction pattern does not show any diffraction rings. Fig. 17 shows the high sensitivity of the UTS to crystalline transition. At the point where the temperature drop occurs, few crystal nucleation sites emerge. Detection of this transition is critical to obtain larger grain size for high quality thin

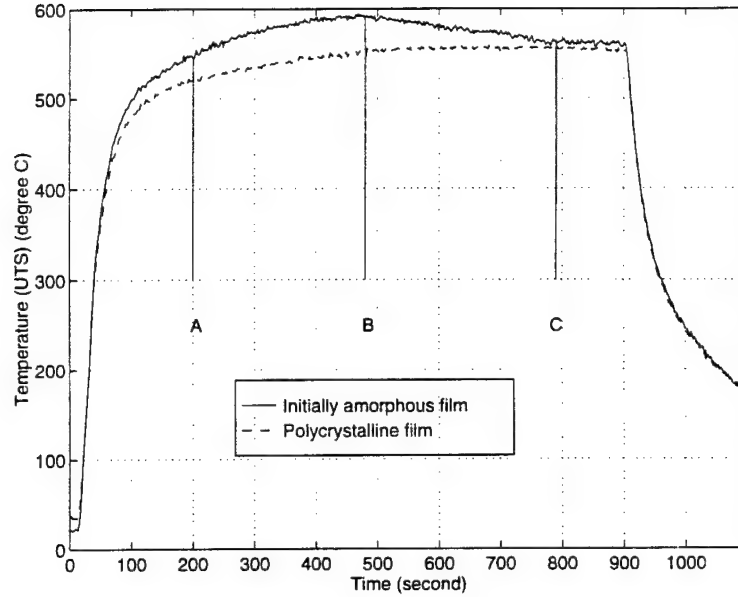


Figure 15: Wafer temperature measured by UTS during the RTA of amorphous silicon on quartz substrate. The wafer is heated two times by the same lamp power recipe without taking it out of the RTM.

film transistors. At point C, the temperature is stable and the films are fully polycrystalline as evidenced in the diffraction pattern.

The feasibility of crystallization monitoring for high quality thin film transistor fabrication is verified by Subramanian et al [23]. A set of 10 cm quartz control wafers are annealed in a conventional furnace at 500°C for 120 hours as control elements. Another set of wafers are first annealed in RTM until point B to create nucleation sites for grain growth using the temperature measurement by the UTS. The wafers are further annealed in the furnace for 24 hours at 500°C for crystallization with large grains. Fig. 19 shows the electron mobility in PMOS thin film transistors produced from these two sets of wafers as a function of radial position on the wafer. The mobility of thin film transistors annealed in RTM using the UTS for endpoint detection is nearly 25% higher than furnace annealed transistors. The mobility is clearly improved especially in the region between 30-45 mm, where the nucleation was nearly completely started. The spatial variation in wafer temperature and mobility can be correlated by temperature tomography which is discussed in the next sections. The UTS clearly provides a unique tool for *in-situ* crystallinity and temperature monitoring during the RTA of thin films on transparent substrates. This enables production of thin film transistors with improved performances with higher throughput.



Figure 16: TEM micrograph of the thin silicon film at point A. The film is still totally amorphous as evidenced in the blurred electron diffraction pattern.

6 In-situ temperature tomography for semiconductor processing

Average temperature is of limited use for multi variable temperature uniformity control purposes. Of more interest is the temperature distribution on the wafer. Using the UTS with a single transmitter-receiver pair gives the average wafer temperature along the path joining the transmitter and receiver. By making measurements on different paths covering the wafer surface and using tomographic reconstruction, real-time temperature distribution on the wafer is obtained. In this section we describe two temperature tomography systems that can be used for clamped and simply supported semiconductor wafers, respectively.

6.1 Temperature tomography with 8 sensors

When the wafer is clamped to a flat surface as in case of many semiconductor process chambers, the number of support pins can be larger than three. In this case, each sensor can



Figure 17: TEM micrograph of the thin silicon film at point B. The small nucleation sites are the centers for grain growth, where the rest of the film is still amorphous.

be individually spring loaded to have a reproducible contact with the wafer. Spring loading also improves the SNR of the system by increasing the area of the Hertzian contacts, and hence the coupling of the acoustic energy to the wafer.

As an application of the UTS in this kind of process chamber, eight quartz pins are used to measure average temperature along different paths covering the whole wafer surface. This was achieved by using one sensor as transmitter and all the others as receivers as shown in Fig. 20, and then sequencing each of the eight sensors as a transmitter. After data acquisition, tomographic reconstruction techniques are used to calculate *in-situ*, wafer temperature distribution. Computer-controlled electronic circuitry was used to multiplex the signals and perform transmit/receive switching between the transducers. For each complete data set, a short electrical pulse is applied to the chosen transducer and the TOF to the other seven sensors are measured. The same acquisition is performed for each sensor by changing the transmitter under computer control; the TOF data is stored in a measurement vector. The receivers are scanned sequentially, resulting in a data acquisition time of 1.4 sec. If a separate counter is used for each receiving channel, the data for each transmitter can be captured during a single excitation cycle, hence the data acquisition time can be reduced to 0.4 sec.

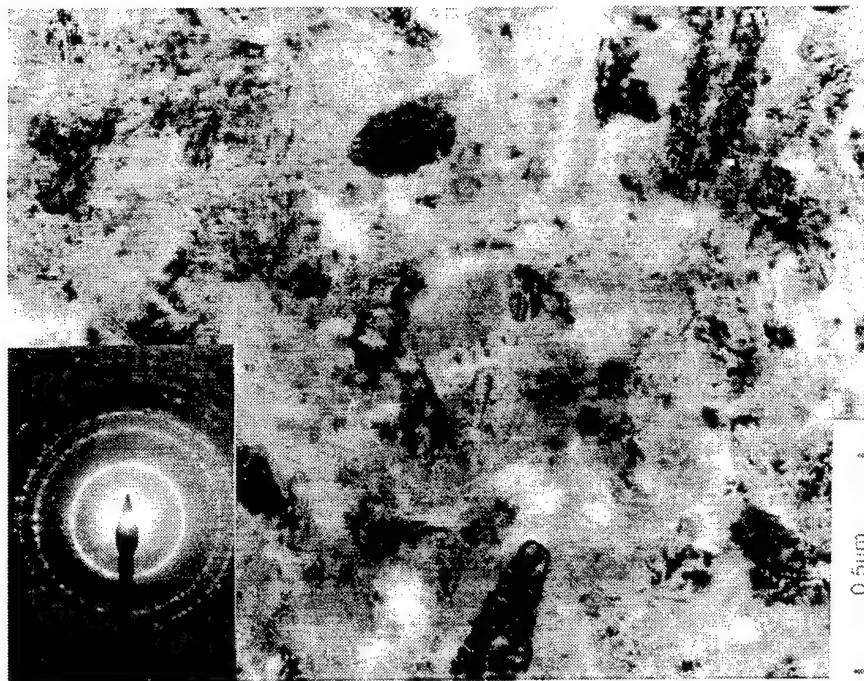


Figure 18: TEM micrograph of the thin silicon film at point C. The film has passed the phase transition everywhere. The sharp diffraction rings indicate the polycrystalline nature of the film.

For tomographic reconstruction, the linear equation solving approach is feasible, since a maximum number of 28 pixel values is to be calculated. Different pixel maps are considered for reconstruction. The projection matrix elements are calculated as the normalized length of the measurement paths in the corresponding pixel, assuming constant acoustic wave velocity, and hence temperature, in each pixel. The inverse of the projection matrix is calculated only once because the geometry was fixed for given pin locations. To compensate for the effect of anisotropy in tomographic reconstruction, a separate calibration is done for each measurement path. The system is used to obtain tomographic temperature images of a 10 cm, 0.5 mm thick, (100) p-type silicon wafer. C-type thermocouples are welded at three different locations of the wafer to provide temperature reference. A 500 W tungsten halogen lamp is used as the heating source. For calibration, TOF data is collected for each measurement path while the wafer temperature is kept steady at different levels, taking the thermocouple readings as a reference. These data points are then used to write the temperature as a third order polynomial of TOF. Image reconstruction is performed as follows: The measurement vector, formed by TOF measurements, is multiplied by the inverse of the projection matrix to get the TOF in each pixel. The actual pixel temperatures are

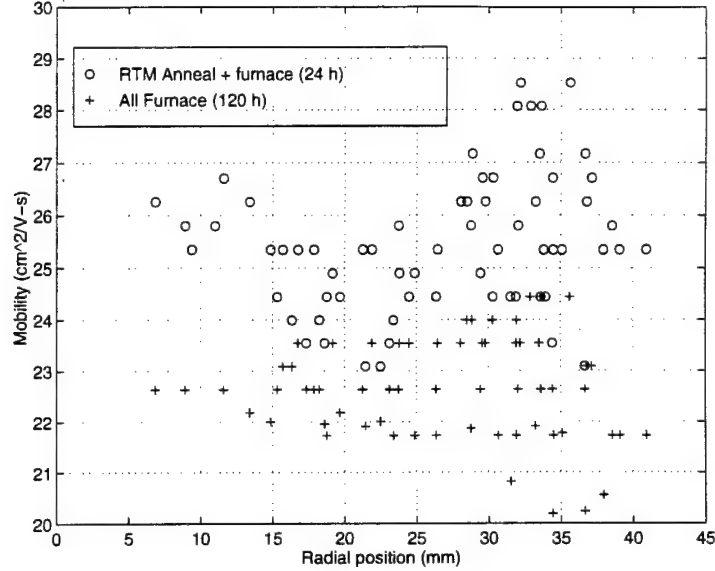


Figure 19: Distribution of the mobility of PMOS thin film transistors on quartz wafers as a function of radial position.

calculated using the polynomials obtained from calibration. Since the algorithm consists of a matrix multiplication and polynomial evaluation, the time required for calculation is negligible as compared to the time of data acquisition. Fig. 21 shows a reconstructed image of the wafer along with the thermocouple locations and readings. In this particular case, the heating lamp is masked in order to get a circularly-symmetric temperature distribution, and circular ring is chosen as the pixel shape. This pixel map is convenient for temperature control of rapid thermal processors having a circularly-symmetric heating lamp structure as in case of RTM [1]. The pixel values were in excellent agreement with thermocouple readings, except for the outermost ring. The error resulting from the assumption of constant temperature across the pixel is proportional to the temperature gradient in that pixel. Since the heat loss from the edge of the wafer is higher as compared to the center, the temperature gradient near the edge is large as observed from the thermocouple readings. This results in loss of accuracy in tomographic reconstruction, especially near the edge. Assuming a 10°C linear temperature variation and a single measurement path across a pixel, the mean error in assigning the average temperature value to the whole pixel is $\pm 5^{\circ}\text{C}$, with a $\pm 2^{\circ}\text{C}$ accuracy in the average measurement. It should be noted that this is the worst case, considering that the error decreases with increasing number of measurement paths used to calculate the pixel value. By incorporating the information obtained from simulation of rapid thermal processors in tomographic reconstruction, and increasing the number of sensors, these errors

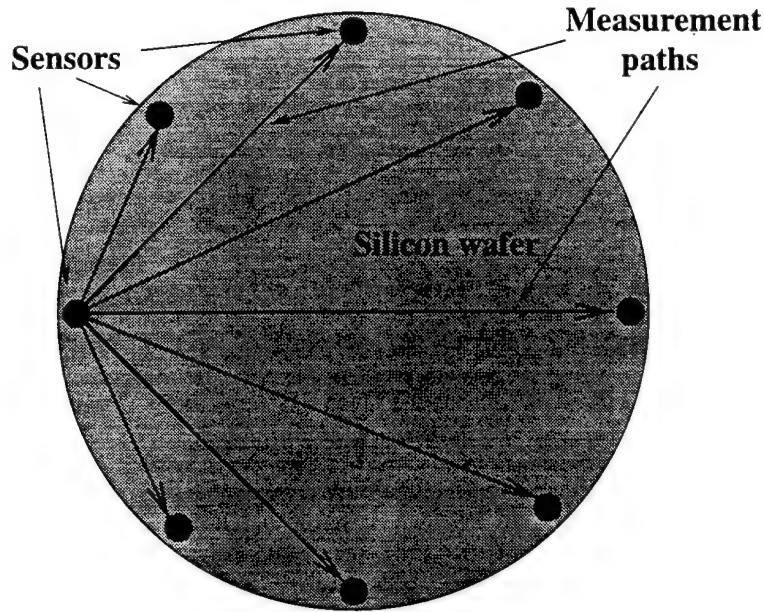


Figure 20: Sensor locations and measurement paths for wafer temperature tomography with 8 sensors.

can be reduced.

6.2 3-Zone temperature tomography

By increasing the number of spring loaded sensors, it is possible to increase the spatial resolution and obtain high SNR. However, in many rapid thermal processing systems, as well as the Stanford RTM, the wafer is simply supported by 3 quartz rods. This limits the number of sensors and the maximum force that can be applied to the Hertzian contacts. Using the first zero crossings for TOF data with three sensors, only three different paths can be used for wafer temperature measurement.

To use the available sensors and the paths to get wafer temperature distribution, a three zone tomography system is developed. Since the RTM has a circularly symmetric heating lamp structure with three independent zones, the temperature zones are also chosen as concentric circles. The following issues are considered in optimizing the zone dimensions and sensor locations:

1. The mechanical stability and high signal to noise ratio,
2. A well conditioned tomographic reconstruction matrix,
3. Insensitivity to wafer alignment.

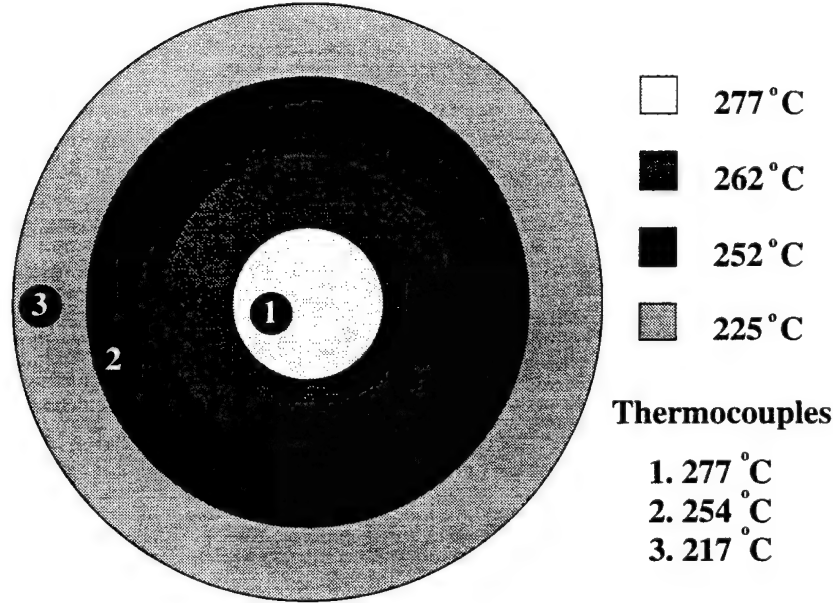


Figure 21: Reconstructed temperature tomography results and the corresponding thermocouple readings for a 10 cm silicon wafer.

As mentioned before, the mechanical stability depends on the force at the Hertzian contacts. In order to get linearly independent measurement paths, the sensors should be placed at angles different than 120° from each other resulting an uneven force distribution, which can be calculated from sensor positions. The reconstruction matrix should consist of linearly independent vectors and should not be ill-conditioned to have noise immunity. The sensor positions and the tomography zone dimensions determine the reconstruction matrix. Wafer alignment is also an issue, because of the anisotropic nature of silicon. The paths directions should be determined to minimize errors due to variations in the wafer orientations. A weighted error function taking these factors into account is constructed and it is minimized using the commercial MATLAB software package. The result of the optimization is approximately sketched in Fig 22. The optimized values obtained for the pixel radii are $r_1 = 0.5337$ and $r_2 = 0.7071$, normalized to wafer radius. The angles are $\theta_1 = 115.8^\circ$ and $\theta_2 = 270^\circ$.

A base plate with the optimized sensor positions was manufactured and computer controlled electronics were implemented to multiplex the transmitter and receiver sensors. Results of an initial experiment with the system is shown in Fig. 23. During the experiment, a 10 cm diameter silicon wafer is used. In the first part of the measurements only the center lamp is used at 80% power and turned off when the wafer temperature is stabilized. The

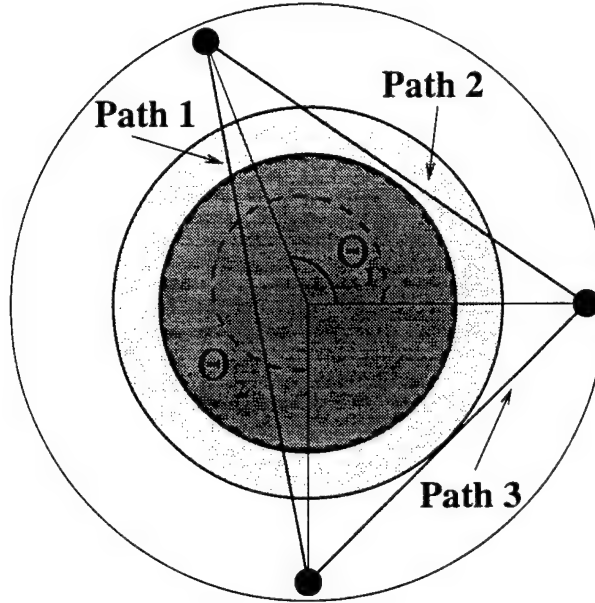


Figure 22: Geometry of the optimized pixels and sensor positions for 3-zone tomography.

procedure is then repeated by the intermediate and outer zones with 50% lamp power. The TOF data is recorded simultaneously at a rate of 10 Hz for the 3 measurement paths. Path 1 is the longest path going through the center zone and it is affected most by turning the center zone of the lamp and path 3 is the shortest path traversing mainly the outermost pixel, and it is affected the least by the center lamp zone. The differences in the TOF variations indicate that, these paths carry independent information that may be used for multi variable closed loop wafer temperature control. The mobility distributions shown in Fig. 19 provides a means to verify the three zone temperature tomography results. This in turn can be utilized to improve uniformity of the RTA of thin film transistors.

7 Conclusion

Our efforts in ultrasonic temperature measurement for semiconductor processing showed that the approach is feasible for real implementations. By monitoring the temperature and thin film crystallization *in-situ* we revealed a unique ability of the ultrasonic temperature sensor. The improved PMOS transducers is just a sign of a new area of applications. We also realized *in-situ* temperature tomography, which is very useful especially for large wafers. The three zone tomography has already begun finding applications in thin film

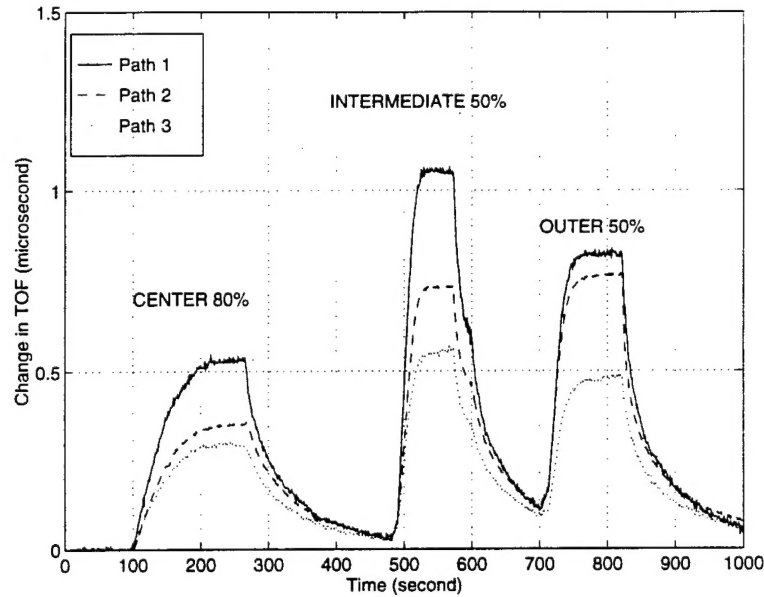


Figure 23: TOF variations of the measurement paths for 3-pin tomography with activation of different zones of the RTM lamp.

crystallization experiments. Our theoretical results on effect of thin films also helped us optimize the *in-situ* temperature and film thickness sensor.

References

- [1] Apte, Pushkar P. and Saraswat, Krishna, C. Rapid thermal processing uniformity using multivariable control of a circularly symmetric 3 zone lamp. *IEEE Transactions on Semiconductor Manufacturing*, 5:180, 1992.
- [2] Bertram Alexander Auld. *Acoustic Fields and Waves in Solids*. Krieger Publishing Co., 1990.
- [3] Bollmann, D. and Habberger, K. Measurement of wafer temperature by interference. *Microelectronic Engineering*, 19:383–88, 1992.
- [4] Dankoski, Paul, Gyugyi, Paul, and Franklin, Gene. An extensible software design applied to rapid thermal processing. In *Rapid Thermal and Integrated Processing II*, pages 183–8, San Francisco, California, April 1993.

- [5] Fiory, A.T., Schietinger, C., and Adams, B. and Tinsley, F.G. Optical fiber pyrometry with in-situ detection of wafer radiance and emittance-Accufiber's ripple method. In *MRS '93 Spring Meeting*, San Francisco, California, April 1993. Material Research Society.
- [6] G. Simmons and H. Wang. *Single crystal elastic constants and calculated aggregate properties: A handbook*. MIT Press, 1971.
- [7] Garland, C.W. and Park, K.C. Low-temperature elastic constants of gallium arsenide. *Journal of Applied Physics*, 161(3):759-60, 1961.
- [8] John J. Hall. Electronic effects in the elastic constants of n-type silicon. *Physical Review*, 161(3):756-61, 1967.
- [9] Bechara Honein. *Wave propagation in submerged piezoelectric composites*. PhD thesis, Stanford University, 1992.
- [10] Kakkad, R., Smith, J., Lau, W.S., and Fonash, S.J. and Kerns, R. Crystallized Si films by low-temperature rapid thermal annealing of amorphous silicon. *Journal of Applied Physics*, 65:2069-72, 1989.
- [11] Yong Jin Lee. *Temperature measurement in Rapid Thermal Processing using acoustic techniques*. PhD thesis, Stanford University, 1994.
- [12] Lee, Yong-Jin, Khuri-Yakub, B.T., and Saraswat, Krishna C. Temperature measurement in rapid thermal processing using acoustic techniques. *Review of Scientific Instruments*, 65(4):974-6, April 1994.
- [13] Lee, Yong-Jin, Khuri-Yakub, B.T., and Saraswat, Krishna C. Temperature measurement in rapid thermal processing using the acoustic temperature sensor. *IEEE Transactions on Semiconductor Processing*, 9(1):115-21, February 1996.
- [14] Lee, Yong-Jin, Khuri-Yakub, B.T., Saraswat, Krishna C., and Moslehi, Mehrdad. Photoacoustic measurements of silicon wafer processing temperatures. In *Ultrasonics Symposium*, Montreal, Canada, October 1989. IEEE Ultrasonics, Ferroelectrics, and Frequency Control Society.
- [15] McSkimmin, H.J. Measurement of elastic constants at low temperatures by means of ultrasonic waves- data for silicon and germanium single crystals, and for fused silica. *Journal of Applied Physics*, 24(8):988-97, August 1953.

- [16] Okada, Yasumada and Tokumaru, Yoza. Precise determination of lattice parameter and thermal expansion coefficient of silicon between 300 and 1500 K. *Journal of Applied Physics*, 56(2):314-20, July 1984.
- [17] Pei, Jun, Degertekin, F. Levent, Stanke, Fred, and Khuri-Yakub, B.T. Simultaneous *in-situ* measurement of film thickness and temperature using ultrasonic waves. In *Ultrasonics Symposium*, pages 413-6, San Antonio, Texas, 1996. IEEE Ultrasonics, Ferroelectrics, and Frequency Control Society.
- [18] Pei, Jun, Degertekin, F. Levent, Khuri-Yakub, B.T., and Saraswat, Krishna C. *In situ* film thickness measurement with acoustic Lamb waves. *Applied Physics Letters*, 66(17):2177-9, April 1995.
- [19] L. Peters. The hottest topic in RTP. *Semiconductor International*, 14(9):56-8, August 1991.
- [20] Peuse, Bruce, Rosekrans, Allan, and Snow, Kenneth. In-situ temperature control of RTP via thermal expansion measurement. In *SPIE Vol. 1804, Rapid Thermal and Laser Processing*, pages 45-54, 1992.
- [21] Fred Roozeboom. Rapid thermal processing: status, problems and options after the first 25 years. In *MRS '93 Spring Meeting*, San Francisco, California, April 1993. Material Research Society.
- [22] Sampson, R.K., Conrad, K.A., and Irene, E.A. and Massoud, H.Z. Simultaneous silicon wafer temperature and oxide film thickness measurement in rapid-thermal processing using ellipsometry. *J. Electrochem. Soc.*, 140(6):1734-43, June 1993.
- [23] Saraswat, Krishna C. et al. Rapid thermal multiprocessing for a programmable factory for adaptable manufacturing of IC's. *IEEE Trans. on Semiconductor Manufacturing*, 7(2):159-75, May 1994.
- [24] Subramanian, Vivek, Dankoski, Paul, Degertekin, F. Levent, Khuri-Yakub, B.T., and Saraswat, Krishna C. Controlled two-step solid-phase crystallization for high performance polysilicon TFTs. *submitted to Electron Device Lett.*, November 1996.
- [25] Subramanian, Vivek, Degertekin, F. Levent, Dankoski, Paul, Khuri-Yakub, B.T., and Saraswat, Krishna C. In-situ monitoring of crystallinity and temperature during rapid thermal crystallization of Si on glass/quartz using an acoustic sensor. *submitted to J. Electrochem. Soc.*, November 1996.
- [26] P.J. Timans. Emissivity of silicon at elevated temperatures. *Journal of Applied Physics*, 74(10):6353-63, November 1993.

- [27] P.J. Timans. The temperature dependence of the emissivity of semiconductors. In *Rapid Thermal Processing '93*, pages 282–86, Scottsdale, Arizona, August 1993.
- [28] P.J. Timans. The effect of coatings on the emissivity of silicon. In *Rapid Thermal Procesing '94*, Monterey, California, August 1994.
- [29] Yudasaka, Ichio and Ohshima, Hiroyuki. Rapid thermal annealing technique for polycrystalline silicon thin-film transistors. *Jpn. J. Appl. Phys.*, 33:1256–60, March 1994.